Photoelectrochemical Cell for Simultaneous Electricity Generation and Heavy Metals Recovery from Wastewater

Dawei Wang [a], Yi Li [a]*, Gianluca Li Puma [b]*, Panagiotis Lianos [c], Chao Wang [a], Peifang Wang [a]

[a] *Key Laboratory of Integrated Regulation and Resource Development of Shallow Lakes, Ministry of Education, College of Environment, Hohai University. Xi Kang Road #1, Nanjing 210098, PR China; E-mail: envly@hhu.edu.cn*

[b] *Environmental Nanocatalysis & Photoreaction Engineering, Department of Chemical Engineering, Loughborough University, Loughborough LE11 3TU, United Kingdom; E-mail: g.lipuma@lboro.ac.uk*

[c] *Department of Chemical Engineering, University of Patras, 26500 Patras, Greece*

* Corresponding authors

Abstract

The feasibility of simultaneous recovery of heavy metals from wastewater (e.g., acid mining and electroplating) and production of electricity is demonstrated in a novel photoelectrochemical cell (PEC). The photoanode of the cell bears a nanoparticulate titania (TiO_2) film capped with the block copolymer [poly(ethylene glycol)-b-poly(propylene glycol)-b-poly(ethylene glycol)] hole scavenger, which consumed photogenerated holes, while the photogenerated electrons transferred to a copper cathode reducing dissolved metal ions and produced electricity. Dissolved silver Ag^{+}, copper Cu^{2+}, hexavalent chromium as dichromate $Cr_2O_7^{2-}$ and lead Pb^{2+} ions in a mixture (0.2 mM each) were removed at different rates, according to their reduction potentials. Reduced Ag^{+}, Cu^{2+} and Pb^{2+} ions produced metal deposits on the cathode electrode which were mechanically recovered, while $Cr_2O_7^{2-}$ reduced to the less toxic Cr^{3+} in solution. The cell produced a current density J_{sc} of 0.23 mA/cm^2, an open circuit voltage V_{oc} of 0.63 V and a maximum power density of 0.084 mW/cm^2. A satisfactory performance of this PEC for the treatment of lead-acid battery wastewater was observed. The cathodic reduction of heavy metals was limited by the rate of electron-hole generation at the photoanode. The PEC performance decreased by 30% after 9 consecutive runs, caused by the photoanode progressive degradation.

Keywords: Photoelectrochemical cell; Wastewater treatment; Heavy metals reduction; Electricity generation.

1. Introduction

Uncontrolled release of heavy metals into water as a result of industrialization is an environmental problem of global concern, which poses significant risk to humans, plants and animals [1,2]. For example, the uncontrolled release of toxic mercury in 1950s and 1960s in Japan from the production of acetaldehyde caused adverse effects to the inhabitants of Minamata, a small fishing and farming village in Japan [3]. Other heavy metals such as cadmium, copper, lead *etc*. from industrial processes (for instance, lead can easily escape into environment by improper handling of lead-acid batteries) are also frequently, threatening the ecosystem [4]. Since most conventional wastewater treatment processes, especially those based on conventional biological methods, are ineffective in removing heavy metals [5], new approaches are necessary in order to develop sustainable solutions.

The rapid industrial development and its long-term sustainability calls for most of heavy metals to be recovered as highly desirable recyclable resources. For this purpose, advanced oxidation processes including photocatalysis have been investigated for the effective removal of metal ions [6-8]. In photocatalysis the absorption of photons by a semiconductor photocatalyst generates electron-hole pairs [9] and in turn highly reactive radical species, which lead to the oxidation of organic wastes [10]. A typical photocatalyst is nanostructured titanium dioxide (TiO_2). Photocatalysis is also a potentially efficient method to recover metals from wastewater, which occurs through the reduction of the dissolved metal ions to their metallic state by interaction with photogenerated electrons, in the presence of a hole

scavenger [11]. However, current laboratory studies have not been translated to real applications in wastewater treatment, since the hole scavengers are often relatively costly reagents such as methanol and $NaHCO_3$ [12] which makes their use unrealistic in industry. Early studies performed with suspensions of nanoparticle photocatalysts [13-16] were not practical, since the separation of the suspended catalyst from the aqueous suspension, and of the metals from the solid, are highly challenging [17]. Clearly, the development of a robust technology to recover metals by photocatalysis requires the immobilized of the photocatalyst on a support to favour the recovery of the deposited metals. The metal reduction process involves the migration of electrons, therefore, it may also be possible to generate electricity during the recovery of metals from the wastewater [18, 19]. Within this contest, the recovery of heavy metals from wastewater by *photoelectrocatalysis* has the potential to simultaneously address three issues, including (1) pollution prevention of heavy metals, (2) metal resources conservation and (3) renewable energy generation.

To address this challenge, in this study we developed a novel photoelectrochemical cell (PEC) carrying a nanoparticulate polymer capped titania photoanode and a Pt cathode (Fig. 1) which were connected by an external circuit. Simultaneous electricity generation and metal recovery was observed when the photoanode was exposed to UV irradiation. The performance and underlying mechanism of this innovating cell for environmental remediation with simultaneous generation of renewable energy are presented in this study. Previous studies in literature utilizing PEC have focused primarily on the removal or organic contaminants [18] and this is one of the few

focusing on the removal and recovery of heavy metals from wastewater with simultaneous production of electricity.

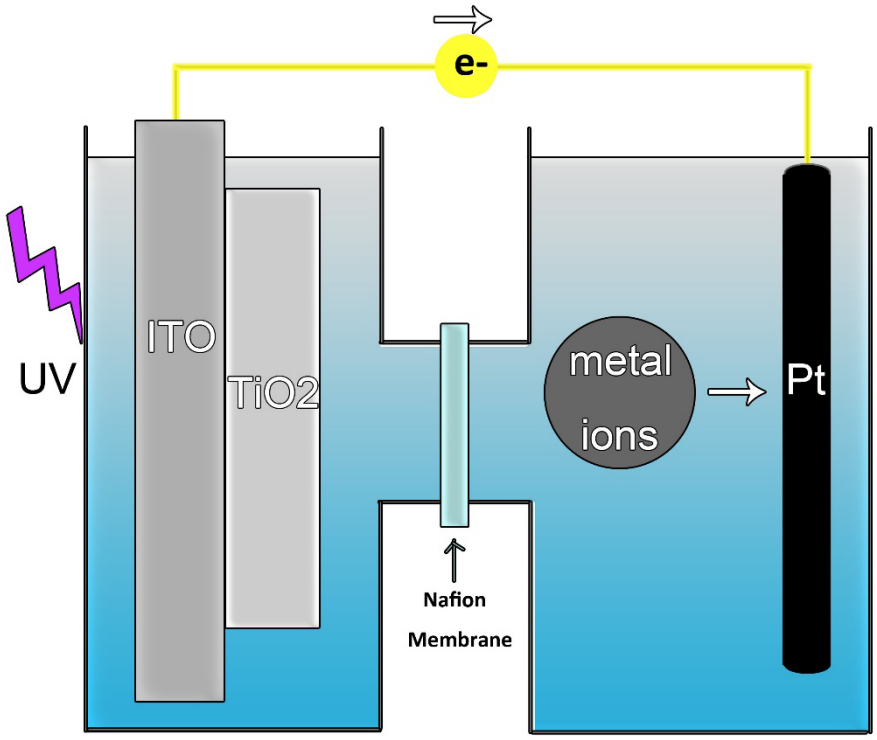

Fig. 1. Schematic illustration of the PEC for the purpose of simultaneous metal recovery and energy production.

2. Experimental

2.1 Chemicals

Titanium chloride ($TiCl_4$), poly(ethylene glycol)-b-poly(propylene glycol)-b-poly(ethylene glycol) (P123), polyvinyl alcohol (PVA, Mw≈22,000) and diethylene glycol (DEG) were obtained from Sigma-Aldrich. Copper sulfate ($CuSO_4$), copper nitrate ($Cu(NO_3)_2$), silver nitrate ($AgNO_3$), silver sulfate (Ag_2SO_4), nickel nitrate ($Ni(NO_3)_2$), nickel sulfate (Ni_2SO_4), lead nitrate ($Pb(NO_3)_2$) and $K_2Cr_2O_7$ were

purchased from Fisher and used as received. ITO glass (2.3 mm of thickness, 2.25 cm^2 of area, 8Ω/sq) from Dyesol Glass was cleaned with 2-propanol and distilled water several times before use. Ultrapure water (18 MΩ cm) was used throughout all the experiments.

2.2 Synthesis of nanoparticulate TiO_2 photoanode

The TiO_2 nanocrystals were synthesized according to a recent study [20]. In brief, a mixture of $TiCl_4$ (1 mL), NH_4OH (1 mL), P123 (0.6 g) and DEG (20 mL) was heated at 220 °C in air with vigorous stirring (600 rpm) for 3h. After cooling down to room temperature, a light-brown mud-like precipitate was obtained upon addition of acetone and centrifugation. Finally, the sample was washed with acetone and ethanol to remove any residual organic species and re-dispersed in 2 mL H_2O. This procedure was repeated multiple times to produce a 18 mL stock solution. The presence of P123 in this synthesis plays a multiple role: it limits the growth of TiO_2 nanocrystals, it caps them and, most importantly, it acts as sacrificial electron donor to scavenge the photogenerated holes [20, 21]. To prepare the photoanode, 6 g of PVA were firstly added into 14 mL of boiled water (100 °C) to produce a viscous liquid. This fluid was added to a mixture of 18 mL stock solution with 25 mL ethanol at 70 °C. After cooling to room temperature, the liquid paste was immobilized on an ITO glass (area 2.25 cm^2) by doctor-blade technique as reported elsewhere [22, 23]. After coating the films were kept in a clean box for 15 min to relax surface irregularities and the residual mechanical stress of the coating. Finally, the photoanode was gradually heated up to

80 °C at 10°C/min, maintained at this temperature for 15 min and then heated up to 500 °C at 10°C/min and maintained for 30 min, then cooled to room temperature in air. The thickness of the film (11 μm) was increased by repeating this doctor-blade technique. To characterize the nanocrystals after the deposition on the photoanode by the doctor-blade method, the film was mechanically scratched from the ITO glass and dispersed in water by sonication. The samples were further washed with ethanol three times to remove PVA, which was introduced during the coating process, and re-dispersed in water prior to TEM grid preparation.

2.3 Characterization

Transmission electron microscopy (TEM) was performed on a JEOL 2011 operated at 200 kV. X-ray diffraction (XRD) patterns were recorded on a Rigaku X-ray diffractometer D/MAX-2200/PC equipped with Cu Kα radiation (40 kV, 20 mA). UV–vis diffuse reflectance spectroscopy was monitored by UV−vis spectrophotometry (HR2000CG-UV-NIR, Ocean Optics). X-ray photoelectron spectroscopy (XPS) results were obtained with PHI 5000C ESCA with Mg *Kα* source operating at 14 kV and 25 mA. The metals deposited on the Pt cathode were recovered by mechanical scratching of the surface and degassed at 200 °C overnight before XPS analysis. The current-voltage was measured as described elsewhere [23]. The metal ion concentrations were measured with an ICP-MS (ZEEnit700) coupled with a HR column (4.6 mm × 75 mm, Waters, USA) and a 432 conductivity detector (Water, USA). The effluent was a solution of KOH (30 mM) at a flow rate of 1.2

mL/min. *J-V* curves were obtained by a Keithley digital SourceMeter (model 2420) coupled with an external bias.

2.4 Metal Recovery and Electricity Generation

Stock solutions of different metal ions (1 M) were prepared by dissolving the metal salts including $CuSO_4$, $Cu(NO_3)_2$, $AgNO_3$, Ag_2SO_4, $Ni(NO_3)_2$, Ni_2SO_4, $Pb(NO_3)_2$ and $K_2Cr_2O_7$ into deionized water. The solutions were kept under vigorous stirring during the experiments, which were conducted at the natural pH of the metal salt solutions. The photoanode and the Pt strip cathode with a dimension of 30 × 5 mm^2 were connected with a commercial copper wire. The experiments were conducted in an H-type photoelectrochemical reactor (Fig. 1) in which the two compartments were separated by a membrane (Nafion 117, Dupont). The photoanode compartment contained 500 ml of distilled water, while the photocathode compartment contained 500 ml of an aqueous solution of metal ions with NaCl (0.5 M) as supporting electrolyte. Prior to irradiation, the reactor was maintained in darkness for 40 min to equilibrate the adsorption of the solution species with the electrodes. To begin the metal recovery process, the photoanode was irradiated with a UV lamp (311 nm peak emission, 300W, emission spectrum shown in Fig. S1, Supplementary Material (SM)) placed 12 cm from the photoanode, providing an incident photon flux of 21.5 W/m^2. The UV photon flux was measured with a microprocessor-controlled radiometer (Cole-Parmer). During the reaction, 2 ml water samples were collected every 10 min to evaluate the residual concentrations of metal ions.

3. Results and discussion

3.1 Characterization of TiO_2

The UV-vis absorption spectrum of the TiO_2 (Fig. 2a) exhibited a strong absorption band from 250 to 375 nm, which lied within the spectrum of the UV radiation source. The band gap energy was calculated to be approximately 3.5 eV (see SM). TEM imaging of the TiO_2 nanocrystals showed an elongated shape with an average size below ~5 nm. The crystalline structure of the TiO_2 nanocrystals was confirmed by X-ray powder diffraction (XRD) analysis (Fig. 2b), with all diffraction peaks being indexed to anatase phase. The significantly broaden diffraction peaks observed indicated low crystallinity and small sizes of the products. The TiO_2 crystal size (3.9 nm) was calculated from the Scherrer's Equation (see SM) and was in accordance with the TEM results [21]. The characterization of the photoanode film by TEM (Fig. S2, SM) showed that both the shape and size of TiO_2 nanocrystals did not change significantly before and after deposition by the doctor blade process.

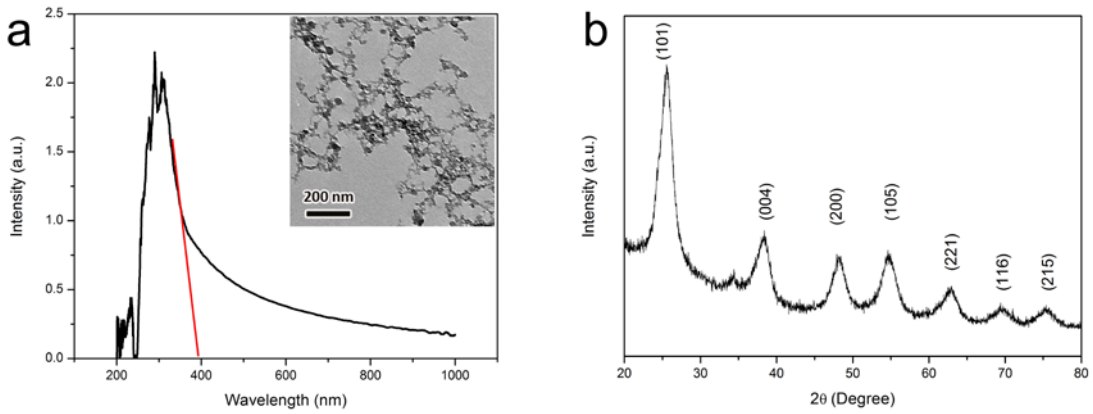

Fig. 2. (a) UV-vis spectrum, the tangent line cross the X axis at 394 nm (cutoff wavelength for band gap calculation); (b) XRD pattern of the as-synthesized TiO_2 nanocrystals, the inset in (a) is the TEM image of TiO_2, scale bar represents 200 nm.

3.2 Metal recovery

3.2.1 Reduction in Single Metal Ion System

Fig. 3a summarizes the residual aqueous metal ion concentrations of Ag^{+}, Cu^{2+}, $Cr_2O_7^{2-}$, Cd^{2+}, Pb^{2+} and Ni^{2+} for experiments performed with a single metal in solution. The photodeposition of the reduced metals on the cathode electrode of the photoelectrochemical cell caused a decrease in the concentration of metal ion in the water. The removal rates varied depending on the nature of the metal and its reduction potential. The concentration of Ag^{+} and Pb^{2+} decreased at the fastest rate, while the change for Cd^{2+} and Ni^{2+} was insignificant. The removal rate of Cu^{2+} was slower than Ag^{+} and Pb^{2+}, but faster than $Cr_2O_7^{2-}$. The conduction band of TiO_2 lies at around -0.2 V and varies slightly with pH [24]. In consequence, the metal ions with a less negative reduction potential than the conduction band of TiO_2 could be reduced at the cathode of the PEC [13]. Table 1 shows that Ag^{+}, Cu^{2+}, $Cr_2O_7^{2-}$, Pb^{2+} could be reduced and that Cd^{2+} and Ni^{2+} encountered thermodynamic limitation, since these ions have more negative reduction potentials than the conduction band of TiO_2. The kinetics of metal ions removal and deposition depends on both the ion charge and the metal reduction potential (i.e., driving force) [25, 26]. Since all experiments were performed under identical experimental conditions and under the same photon flux at the photoanode, the rate of electron-hole generation over the TiO_2 could be considered to be the invariant [27]. The removal rate of metal ions will therefore be favored for those ions that consume less electrons and with a positive electrochemical driving force [25]. A

faster removal of Ag^+ than $Cr_2O_7^{2-}$ was therefore observed, since the reduction of Ag^+ requires one electron while $Cr_2O_7^{2-}$ consumes six electrons. However, different removal performances of lead and copper were observed regardless of their identical valence, which may be attributed to their different conductivities. The deposition of lead over the cathode will make it less conductive, hindering the photocatalytic reduction of lead.

The nature of the products deposited over the Pt strip were analyzed by XPS to elucidate the reduction mechanism of the metals. Fig. 3b, 3c and 3d show the presence of metallic Ag, Cu and Pb in the studied deposits [9, 28, 29]. The reduction of $Cr_2O_7^{2-}$ did not yield a solid product and converted to the less toxic Cr^{3+} ion during the reaction process (as shown by ICP) which remained in solution at acidic pH. The recovery rate of metals from the wastewater was estimated by analyzing the data presented in Fig. 3a. Approximately 80% removal Ag and Pb, and 60% for Cu was obtained after 60 min, while 40% of $Cr_2O_7^{2-}$ was reduced into Cr^{3+}.

Table 1. Redox potentials of metal ions (calculated according to Nernst Equation (pH=3.0) [30]

Electrode reaction	E^0/V
$Cd^{2+} + 2e^- \rightarrow Cd$	-0.40
$Ni^{2+} + 2e^- \rightarrow Ni$	-0.24
$Pb^{2+} + 2e^- \rightarrow Pd$	-0.13
$Cu^{2+} + 2e^- \rightarrow Cu$	0.34
$Ag^+ + e^- \rightarrow Ag$	0.80
$Cr_2O_7^{2-} + 14H^+ + 6e^- \rightarrow 2Cr^{3+} + 7H_2O$	0.88

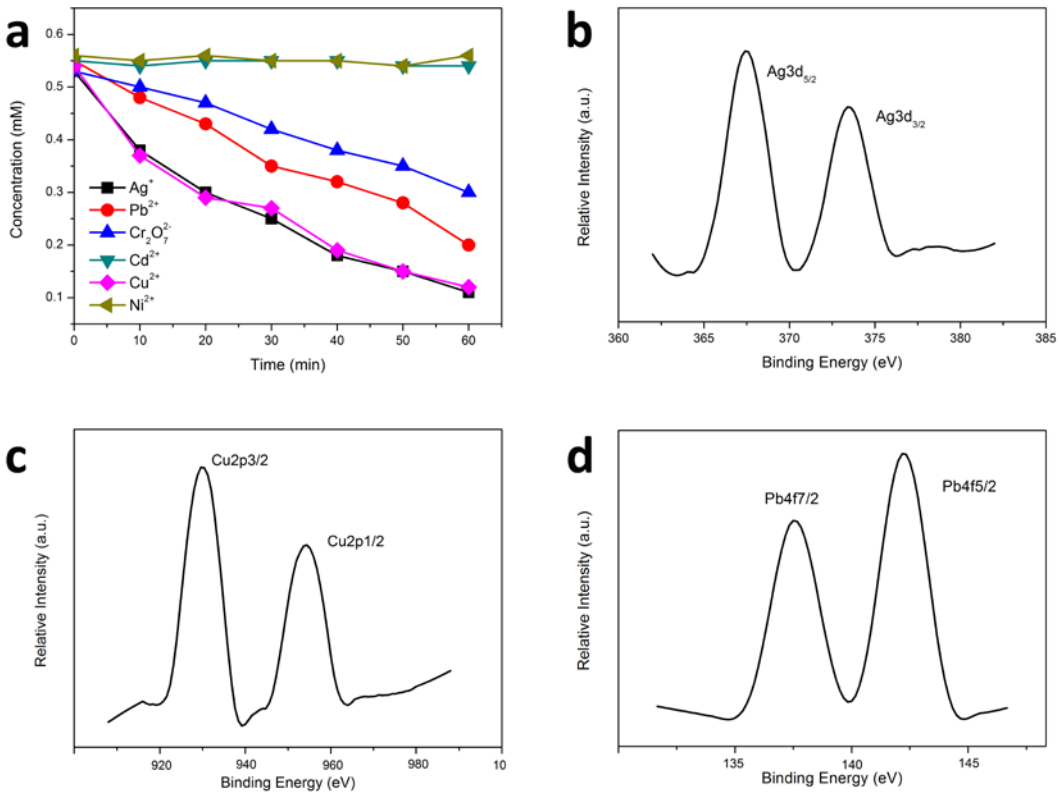

Fig. 3. (a) Photocatalytic reduction of Ag^{+}, Cu^{2+}, $Cr_2O_7^{2-}$, Cd^{2+}, Pb^{2+} and Ni^{2+} in single ion experiments in the cell; (b, c and d) corresponds to the XPS spectrum of the products scratched from the cathode for the photocatalytic reduction of Ag^{+}, Cu^{2+} and Pb^{2+}, respectively. The peaks indicate that the three metal ions were reduced into their metallic form.

3.2.2 Metal Reduction in Complex Water Matrix System

Multiple metal ion aqueous solutions of Ag^{+}, Cu^{2+}, $Cr_2O_7^{2-}$ and Pb^{2+} containing 0.2 mM of each metal (pH=3.0) were prepared to demonstrate the practical application of the PEC for water treatment. The competing reduction reactions at the Pt cathode favored the reduction of the metal ions with the more positive reduction potential. Therefore, $Cr_2O_7^{2-}$ was firstly reduced until totally consumed and this was in a sequence followed by the reduction of Ag^{+} until consumed, then Cu^{2+} until consumed and finally Pb^{2+} (Fig. 4a). In spite of the competition for electrons among these metal ions, all of them were reduced within 160 min of treatment.

Dissolved oxygen (DO) in the water may also have a significant effect on the photoreduction of metal ions [31], because it competes with metal reduction by reacting with photogenerated electrons (Reaction 1) [30]:

$$O_2 + 4H^+ + 4e^- \rightarrow 2H_2O \quad E^0 = 0.99V \text{ pH} = 3.0 \qquad (1)$$

The redox potential was calculated according to Nernst equation. The metal ion aqueous solutions were therefore purged with N_2 or O_2 to reach a saturation state and thus investigate the effect of DO on the reduction of the metal ions. The results were compared with those obtained without purging the solution (blank experiment, Fig. 4a). The results in Fig. 4b show the adverse effect of DO on the removal of both Cu^{2+} and Pb^{2+}, which display a 12.5% removal of Cu^{2+} under O_2 saturated condition within 160 min. On the contrary, the removal was complete in a N_2 saturated atmosphere or in the blank experiment (Fig. S3, SM). Oxygen hindered Cu^{2+} and Pb^{2+} reduction as a result of their relatively high-lying redox potentials (Table 1) that do not provide enough driving force to move electrons, the latter being consumed by oxygen reduction. However, the presence of oxygen did not affect reduction of Ag^+ and $Cr_2O_7^{2-}$ although both ions have lower reduction potentials than oxygen. This behavior has been shown elsewhere [13] and may result from the relatively low solubility of oxygen (~8 mg/L at saturation state). In consequence, the numbers of available electrons are sufficiently plentiful to reduce Ag^+ and $Cr_2O_7^{2-}$ after the total consumption of oxygen, while the reduction of Cu^{2+} and Pb^{2+} was inhibited by the lack of electrons. As a result, oxygen will only play an insignificant role on the performance of the cell due to its negligible solubility.

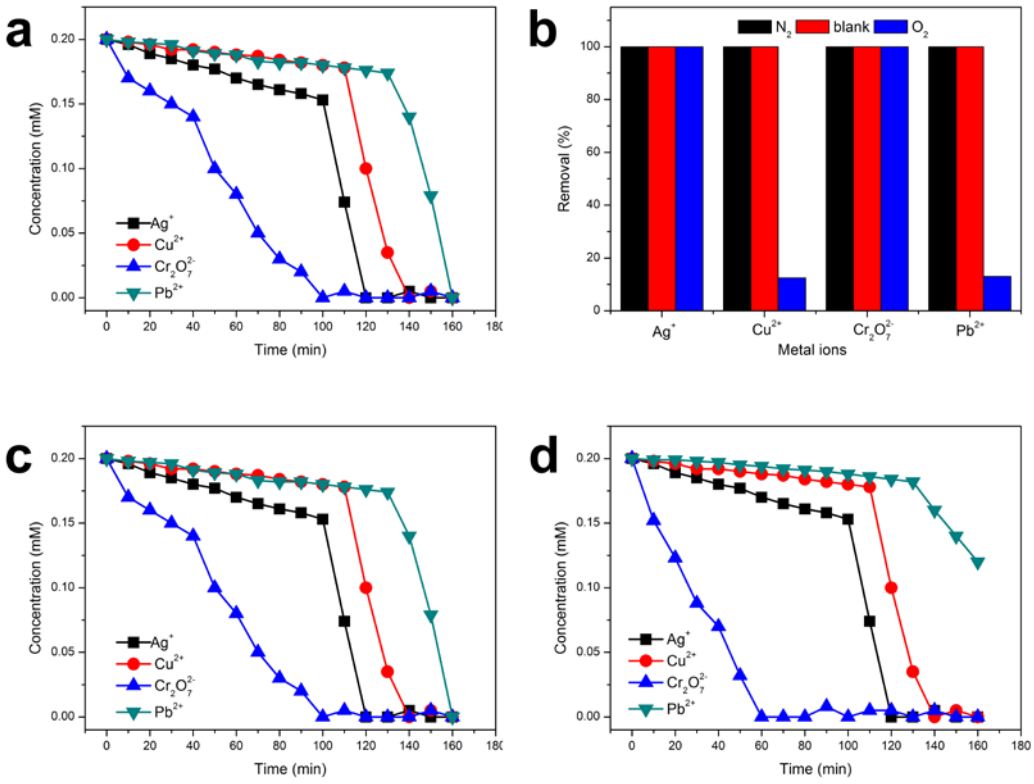

Fig. 4. The removal of Ag^{+}, Cu^{2+}, $Cr_2O_7^{2-}$ and Pb^{2+} under different conditions: (a) the blank experiment, Ag^{+}, Cu^{2+} and Pb^{2+} were added as their nitrate salts while the experiment was conducted with no injection of N_2 or O_2 and no control of pH (~3.0); (b) the effect of N_2 and O_2 on the removal of these four metal ions while other conditions are the same with the blank experiment, the data was recorded at 160 min; (c) the pH was tuned to be ~2.0 by adding HNO_3 while other conditions were the same as in the blank experiment; (d) metal ions were added as sulfate salts, the pH was tuned to ~2.0 by adding H_2SO_4, other conditions were the same as in the blank experiment.

To avoid potentially complex reactions between the metal ions and the introduced anions, only NO_3^{-} or SO_4^{2-} metal salts were used throughout the experiments. In the blank experiment, all the metal ions except $Cr_2O_7^{2-}$ were added as their nitrate salts. Considering that most wastewaters with heavy metal ions are usually acidic (for example, the pH can be as low as ~2.2 in some acid mine drainage systems [32], we further tuned the pH to ~2.0 by adding HNO_3 to mimic the condition of real acid mining wastewater effluents. Under these conditions, with the exception of $Cr_2O_7^{2-}$,

which exhibited a faster removal rate, Ag^{+}, Cu^{2+} and Pb^{2+} experienced an inhibitory effect at lower pH (Fig. 4c). The faster removal of $Cr_2O_7^{2-}$ occurred from the conversion of Cr^{6+} to Cr^{3+}, which is favored at lower pH (higher concentration H^{+} in the reduction reaction shown in Table 1) since the redox potential of $Cr_2O_4^{2-}/Cr^{3+}$ (1.02 at pH 2.0) was higher than the reduction potential of NO_3^{-}/NO (Reaction 2).

$$NO_3^- + 4H^+ + 3e^- \rightarrow NO + 2H_2O \; E = 0.82 \; V \;\; pH = 2.0 \qquad (2)$$

In contrast, the inhibitory effect of NO_3^{-} on Ag^{+}, Cu^{2+} and Pb^{2+} can be attributed to the higher redox potential of NO_3^{-}/NO, although it is comparable to the reduction potential of Ag^{+}/Ag^{0} (Reaction 2 and Table 1). However, the reduction rate of Ag^{+} in the presence of NO_3^{-} was slower than in its absence and only about half of Cu^{2+} and 20% of Pb^{2+} were reduced within 160 min, while in the absence of NO_3^{-} both Cu^{2+} and Pb^{2+} were totally removed. As a result, electrons would preferentially reduce NO_3^{-}, displaying an inhibitory effect on the removal of Ag^{+}, Cu^{2+} and Pb^{2+} metal ions.

Replacing the nitrate metal salts with their sulfate species, produced different results (Fig. 4d). Sulfate anions may be reduced according to the half reaction:

$$SO_4^{2-} + 4H^+ + 2e^- \rightarrow H_2SO_3 + H_2O \; E = -0.08 \; V \; pH = 2.0 \qquad (3)$$

However, since the reduction potential for this reaction is relatively low, only the reduction of Pb^{2+} was retarded by the competition with sulfate anions, while no effect was recorded on the reduction of Cu^{2+} and Ag^{+} that have more positive reduction potentials. The removal rate of $Cr_2O_7^{2-}$ still increased due to the lower pH as explained earlier. In summary, the performance of the PEC in a complex water matrix system suggested that the removal of heavy metals from wastewaters with higher

sulfate content and low nitrate will be favored.

3.3 Electricity Generation and Reaction Mechanism

The direct conversion of solar energy into chemical energy during a wastewater treatment process is attractive with regards to the sustainability and green credentials of water treatment [33]. For this reason, the electricity generated during the recovery process of heavy metals may achieve the goal of converting renewable solar energy into chemical energy with simultaneous recycle of metal resources. The electrical performance of the PEC was evaluated by monitoring the current-voltage (*J-V* plot) and voltage-power density (*V-P* plot) generated during the reduction of the heavy metals. At the beginning of the reaction (0 min), the current intensity J_{sc} was 0.23 mA/cm^2 (calculated according to the area of photoanode), the cell voltage V_{oc} was 0.63 V and the maximum power density was 0.084 mW/cm^2 (Fig. 5a). The photo-electricity conversion efficiency was calculated to evaluate the photoelectrical performance of the PEC (Eq. 4)

$$\text{Efficiency} = \frac{J_{max}V_{max}}{P_{light}} \qquad (4)$$

where J_{max} is the maximum value at short current, V_{max} is the maximum value at open voltage, and P_{light} is the power density of the incident light.

An efficiency of 3.33% was recorded at 0 min, indicating 3.33% of the incident light energy was converted into electricity. However, after 160 min when all the four metal ions were completely removed, the electrical current became negligible as expected. The proposed reaction mechanism in the PEC follows the initial generation of

electron-hole pairs upon irradiation of the photoanode with UV light. The holes are consumed by the polymer (P123) that is capped on the surface of TiO_2 while the electrons are transferred to the cathode where they reduce the dissolved metal ions [21]. The metal ions serve as device electrolyte in this mechanism. As a result, no current was detected when all metal ions were completely removed from the water. Therefore, the cell can generate electricity as long as UV irradiation and metal ions are available.

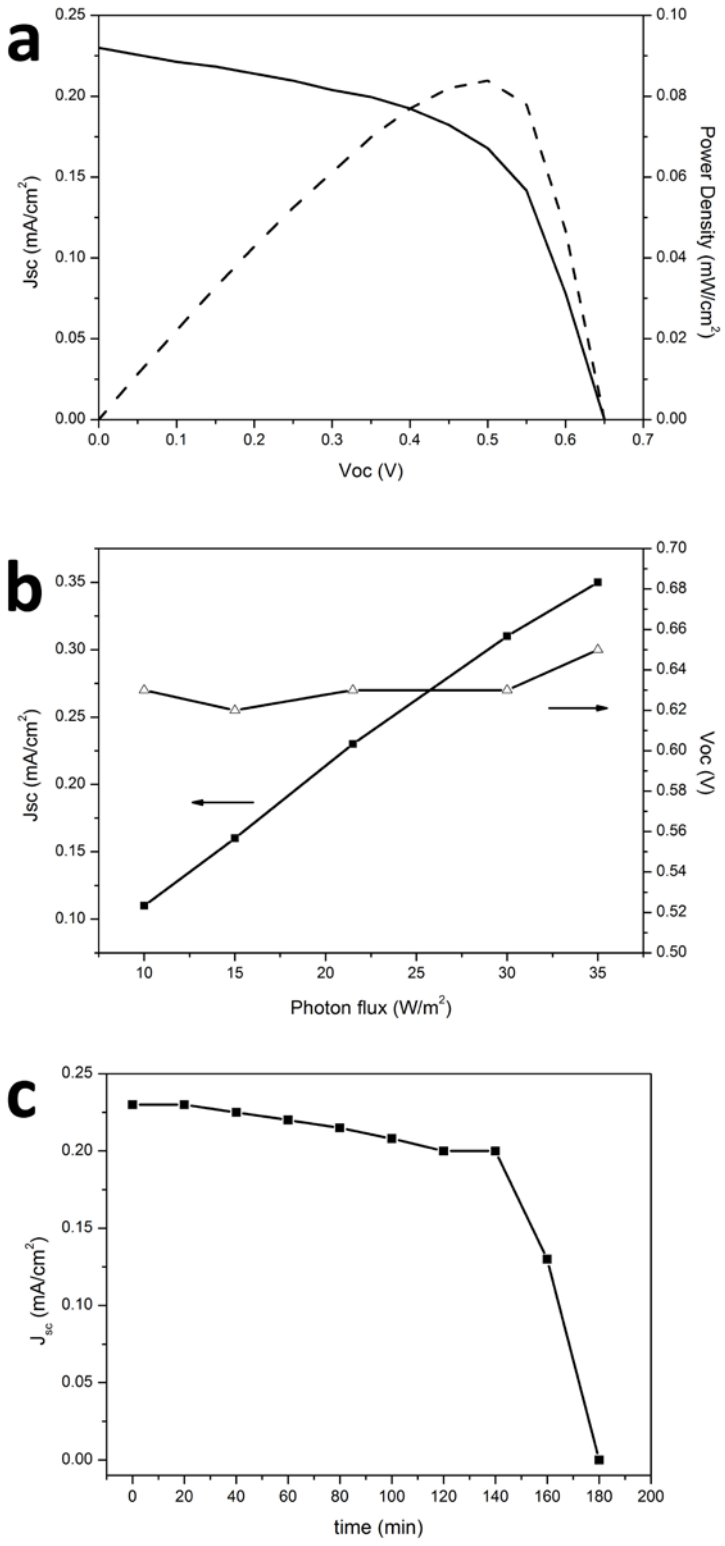

Fig. 5. The electrical performance of the PC: (a) *J-V* plot and *P-V* plot measured at 0 min with an incident photon flux of 21.5 W/m^2; (b) the effect of light intensity on J_{sc} (■) and V_{oc} (△) which were measured at 0 min; (c) the J_{sc} plot as a function of the time of UV irradiation. All the curves were recorded under the blank experiment condition (the concentrations of the four metal ions equal to 0.2 mM).

The incident photon flux and the concentrations of metal ions were further tuned to elucidate the mechanism of electricity generation. The photocurrent J_{sc} depends on both the rate of electron-hole generation on the TiO_2 semiconductor photoanode and the rate of metal reduction at the cathode, and as a result, one of these two factors may be the rate limiting. Varying the concentration (from 0.2 to 5 mM) of metal ions did not influenced the electrical performance of the PEC (data not shown) suggesting that metals ions in solution were always in excess and that the metals reduction process was controlled by the rate of electron-hole charges generation at the photoanode [27]. This was further evidenced by the observed linear dependence of the short current J_{sc} with the incident photon flux (Fig. 5b) suggesting that the photoanode operated in an unsaturated condition with regards to the rate of photon absorption. This also suggested that the reduction process at the photoanode was not controlled by the rate of mass transfer of metal ions to the surface of the cathode. The cell voltage V_{oc} remained effectively constant at 0.63 V since the voltage is known to be influenced by the properties of photoanode material [34], which in our experiments did not vary. The phorocurrent J_{sc} decreased when the metal ions in solution become limiting, after their concentration decreased to such a level to become insufficient to maintain the migration of electrons [35] (Fig. 5c) and the stability of the PEC as discussed below. The steep decline in the electrical current observed at 140 min should be attributed to the combination of these two main controlling factors.

We also investigated the performance of the PEC by replacing the artificial wastewater with real wastewater from a lead battery manufacturing unit in Jiangsu

Province, China (the wastewater characteristics are shown in table 2). A high concentration of SO_4^{2-} was observed because the electrolyte in the lead battery is usually H_2SO_4. As discussed above, since the pH value of the wastewater was 2.3, SO_4^{2-} was reduced to H_2SO_3 prior to the reduction of Pb^{2+} (Fig. S4a, SM). Both the SO_4^{2-} and Pb^{2+} were totally removed after 90 min, which was accompanied by a pH increase to 6.4. Moreover, a V_{oc} of 0.63 V and a J_{sc} with a maximum value of 0.21 mA/cm^2 were also recorded (Fig. S4b, SM). The removal and recovery of the metal ions, the production of electricity and the simultaneous increase in pH suggests the potential use of the proposed PEC for the treatment of wastewater from lead-acid battery industry. It should also be noted that the PEC posed a satisfactory performance in the removal of Pb^{2+} in the presence of the suspended solids, as the photoelectrical performance was comparable to that of observed with artificial wastewater. This could be a further advantage of this PEC in comparison to systems employing suspended photocatalysts, since in the latter case the suspended TiO_2 solid might reduce the overall rate of photon absorption, resulting in an impaired performance of the cell [27, 36].

Table 2. Characteristics of wastewater from a lead battery manufacturing unit

Parameters	Values
pH	2.3
Pb	25 mg/L
Suspended solids	125 mg/L
COD	80 mg/L
SO_4^{2-}	260 mg/L

3.4 Cell stability and reuse

The current intensity decreased slightly even when sufficient metal ions were available within the system, an effect that may be attributed to the stability of the PEC. As a result, the long-term stability and reuse of the cell was investigated to determine potential inactivation mechanisms at the photoanode and/or cathode. The performance of the PEC was recorded for nine consecutive cycles for the reduction of Cu^{2+} alone, which was used to simplify the system. Both the photoanode and cathode were not treated between different cycles, while the concentration of Cu^{2+} was maintained at the same level (~0.5 mM) at the beginning of each cycle. As shown in Fig. 6a, Cu^{2+} was completely removed within 30 min in the first cycle. However, only about 70% of copper metal ion was removed at the end of the 9^{th} cycle, indicating that some inactivation at the photoanode or cathode occurred [37, 38]. The inactivation of the photoanode may be associated with the depletion of P123, which served as hole scavenger under continuous UV irradiation [21]. As previously observed by XPS, metallic Cu deposited on the cathode after the reduction of Cu^{2+}. Consequently, the deposition of metal on the cathode could have also contributed to the inactivation of the performance of the cell. To distinguish whether the inactivation occurred at the photoanode and/or at cathode, further consecutive experiments were carried out using a new photoanode in the PEC before each new cycle started, while the cathode remained invariant. Fig. 6b does not show inactivation in multiple runs, confirming that the accumulation of copper at the cathode did not contribute to a change in performance of the cell, while most likely the inactivation of the cell was caused by

the depletion of P123 at the photoanode. The inactivation of the photoanode also affected the electrical performance of the cell, since the generation rate of electrons at the photoanode decreases with cell cycle, as shown by the continuous decrease of current density in the stability test (Fig. 6c).

A similar experiment was also carried out to check the stability of the PEC with the above-mentioned lead battery wastewater. As shown in Fig. S5a (SM), both Pb^{2+} and SO_4^{2-} were completely removed within 80 min in the first cycle, while almost 68% of lead and sulfate ions were removed in the ninth cycle. The current density after the ninth cycle decreased by approximately 21%, while no significant change of the open voltage was observed. As a result, the performance of PEC applied to the treatment of real wastewater was close to that observed with artificial wastewater, suggesting the potential use of this technology in industry. However, further optimization studies on the stability of the TiO_2 nanocrystals would be required to maintain the performance of the cell over multiple cycles. It is also significant that metals could be directly collected by mechanical scratching of the cathode surface after the completion of the reduction process of the metal ions, indicating this innovative PEC may be able to recover heavy metals from wastewater through a robust and practical method while generating electricity.

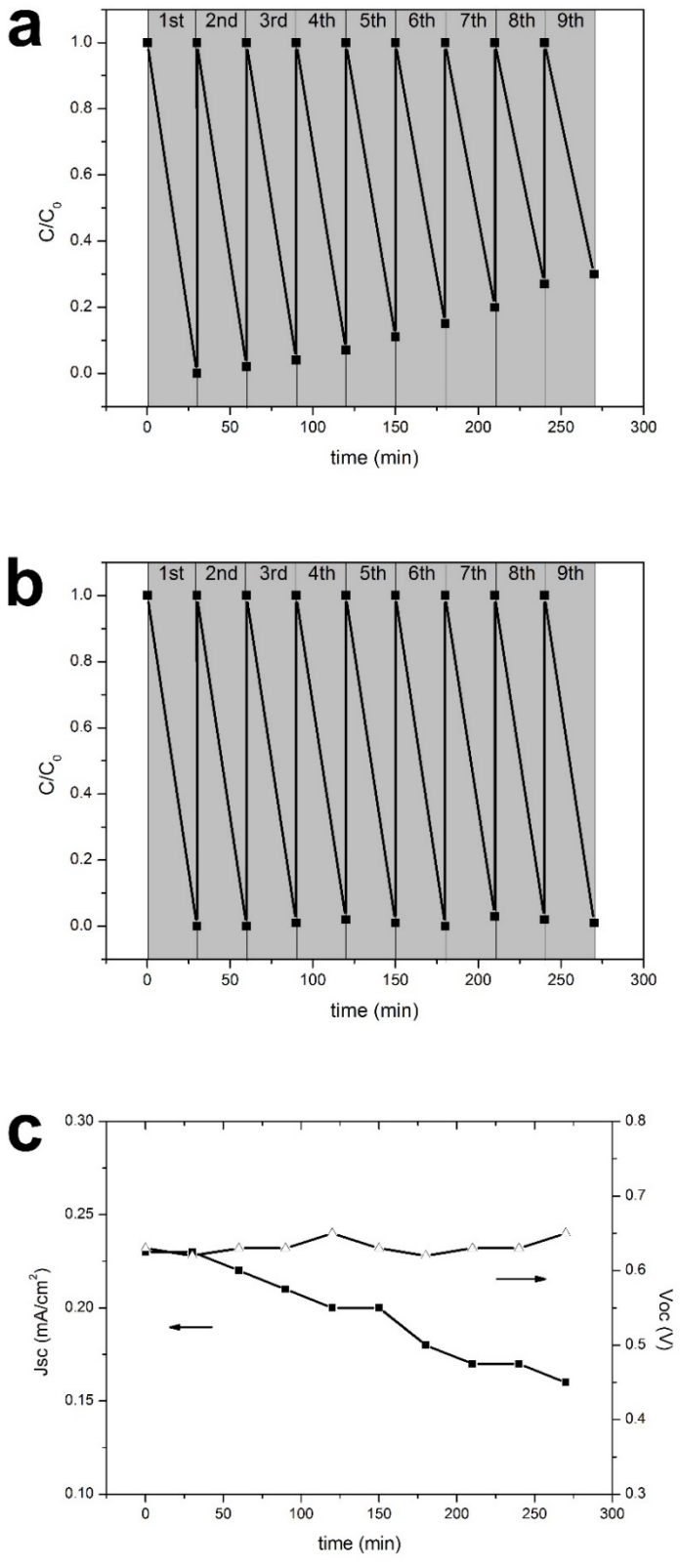

Fig. 6. (a) The removal of Cu^{2+} was recorded continuously for 9 cycles; (b) the removal of Cu^{2+} was recorded with the photoanode being replaced by a new one each cycle; (c) *J-V* corresponds to the cycle test in (a).

4. Conclusions

In this study, we have demonstrated a novel photoelectrochemical cell, which can simultaneously recover metal ions from wastewater and generate electricity. The photoanode of the cell was produced by depositing a layer of polymer capped TiO_2 on ITO glass. Upon irradiation, the photogenerated electrons transferred to the cathode to reduce dissolved metal ions, while the polymer layer capping the TiO_2 consumed the corresponding holes. Electricity was produced and heavy metals were recovered by mechanical scratching of the cathode surface. This demonstration study opens up new opportunities for producing renewable energy from the recovery of heavy metal from wastewater including wastewater from acid mining and the lead-acid battery industry. Although the cell studied here presents some limitations including relatively low electricity generation, the need of UV activation and the relatively low stability, there are significant opportunities for further improvement in both the cell configuration and the photoanode material. Elemental doping of the TiO_2 and the presence of co-catalyst, which have been well established in material science, may provide the key to further improve the photoelectrical performance and the stability of the cell even under visible solar light irradiation.

Acknowledgement

The study was financially supported by the Foundation for Innovative Research Groups of the National Natural Science Foundation of China (51421006), the National Natural Science Foundation of China (51322901 and 51479066), the Research Fund for innovation team of Ministry of Education (IRT13061), the Fundamental Research Funds for the Central Universities (No. 2014B02914, 2015B02114 and 2014B07614), and the Priority Academic Program Development of Jiangsu Higher Education Institutions.

Reference

[1] P. M. Bolger, B. A. Schwetz, Mercury and Health, N. Engl. J. Med. 347 (2002) 1735–1736.

[2] T. W. Clarkson, L. Magos, G. J. Myers, The toxicology of mercury-current exposures and clinical manifestations, N. Engl. J. Med. 349 (2003) 1731–1737.

[3] J. Hightower, Diagnosis Mercury: Money, Politics and Poison, Island Press, (2008). p. 77

[4] T.J. van der Kuijp, L. Huang, C.R. Cherry, Health hazards of China's lead-acid battery industry: a review of its market drivers, production processes, and health impacts, Environ. Health: A Global Access Sci. Source 12 (2013) 61.

[5] C. Das, P. Patel, S. De, S. Dasgupta, Treatment of tanning effluent using nanofiltration followed by reverse osmosis, Sep. Purif. Technol. 50 (2006) 291-299.

[6] J.J. Testa, M.A. Grela, M.I. Litter, Heterogeneous Photocatalytic Reduction of Chromium(VI) over TiO_2 Particles in the Presence of Oxalate: Involvement of Cr(V) Species, Environ. Sci. Technol. 38 (2004) 1589-1594.

[7] H. Yu, S. Chen, X. Quan, H. Zhao, Y. Zhang, Fabrication of a TiO_2-BDD heterjunction and its application as a photocatalyst for the simultaneous oxidation of an Azo dye and reduction of Cr (VI), Environ. Sci. Technol. 42 (2008) 3791-3796.

[8] R. Mu, Z. Xu, L. Li, Y. Shao, H. Wan, S. Zheng, On the photocatalytic properties of elongated TiO_2 nanoparticles for phenol degradation and Cr(VI) reduction, J. Hazard. Mater. 176 (2010) 495-502.

[9] D. Wang, Y. Li, G. Li Puma, C. Wang, P. Wang, W. Zhang, Q. Wang, Ag/AgCl@ helical chiral TiO_2 nanofibers as a visible-light driven plasmon photocatalyst, Chem. Commun. 49 (2013) 10367-10369.

[10] J. Schneider, M. Matsuoka, M. Takeuchi, J. Zhang, Y. Horiuchi, M. Anpo, D.W. Bahnemann, Understanding TiO_2 Photocatalysis: Mechanisms and Materials, Chem. Rev. 114 (2014) 9919-9986.

[11] L. Wang, N. Wang, L. Zhu, H. Yu, H. Tang, Photocatalytic reduction of Cr(VI) over different TiO_2 photocatalysts and the effects of dissolved organic species, J.

Hazard. Mater. 152 (2008) 93-99.

[12] C. Hu, T. Peng, X. Hu, Y. Nie, X. Zhou, J.H. Qu, H. He, Plasmon-Induced Photodegradation of Toxic Pollutants with Ag−AgI/Al_2O_3 under Visible-Light Irradiation, J. Am. Chem. Soc. 132 (2010) 857-862.

[13] D. Chen, A.K. Ray, Removal of toxic metal ions from wastewater by semiconductor photocatalysis, Chem. Eng. Sci. 56 (2001) 1561-1570.

[14] R. Vinu, G. Madras, Kinetics of Simultaneous Photocatalytic Degradation of Phenolic Compounds and Reduction of Metal Ions with Nano-TiO_2, Environ. Sci. Technol. 42 (2008) 913-919.

[15] Y.C. Zhang, J. Li, M. Zhang, D.D. Dionysiou, Size-Tunable Hydrothermal Synthesis of SnS2 Nanocrystals with High Performance in Visible Light-Driven Photocatalytic Reduction of Aqueous Cr(VI), Environ. Sci. Tech. 45 (2011) 9324-9331.

[16] W. Liu, J. Ni, X. Yin, Synergy of photocatalysis and adsorption for simultaneous removal of Cr(VI) and Cr(III) with TiO_2 and titanate nanotubes, Water Res. 53 (2014) 12-25.

[17] M. Chong, B. Jin, C.W.K. Chow, C. Saint, Recent developments in photocatalytic water treatment technology: a review, Water Res. 44 (2010) 2997-3027.

[18] P. Lianos, Production of electricity and hydrogen by photocatalytic degradation of organic wastes in a photoelectrochemical cell: The concept of the Photofuelcell: A review of a re-emerging research field, J. Hazard. Mater. 185 (2011) 575-590.

[19] G. Kim, E.T. Igunnu, G.Z. Chen, A sunlight assisted dual purpose photoelectrochemical cell for low voltage removal of heavy metals and organic pollutants in wastewater, Chem. Eng. J. 244 (2014) 411-421.

[20] W. Wang. N. Xie, L. He, Y. Yin, Photocatalytic colour switching of redox dyes for ink-free light-printable rewritable paper, Nature Commun. 5:5459 doi: 10.1038/ncomms6459 (2014).

[21] W. Wang, M. Ye, L. He, Y. Yin, Nanocrystalline TiO_2-Catalyzed Photoreversible Color Switching, Nano Lett. 14 (2014) 1681-1686.

[22] I. Grčić, G. Li Puma, Photocatalytic degradation of water contaminants in multiple photoreactors and evaluation of reaction kinetic constants independent of photon absorption, irradiance, reactor geometry, and hydrodynamics, Environ. Sci. Technol. 47 (2013) 13702-13711.

[23] D. Wang, Y. Li, G. Li Puma, C. Wang, P. Wang, W. Zhang, Q. Wang, Dye-sensitized photoelectrochemical cell on plasmonic Ag/AgCl @ chiral TiO_2 nanofibers for treatment of urban wastewater effluents, with simultaneous production of hydrogen and electricity, Appl. Catal. B. Environ. 168 (2015) 25-32.

[24] M.D. Ward, J.R. White, A.J. Bard, Electrochemical investigation of the energetics of particulate titanium dioxide photocatalysts. The methyl viologen-acetate system, J. Am. Chem. Soc. 105 (1983) 27-31.

[25] J. Halpern, G. Czapski, J. Jortner, G. Stein, Mechanism of the Oxidation and Reduction of Metal Ions by Hydrogen Atoms, Nature 186 (1960) 629-630

[26] H.C. Choi, M. Shim, S. Bangsaruntip, H. Dai, Spontaneous Reduction of Metal Ions on the Sidewalls of Carbon Nanotubes, J. Am. Chem. Soc. 124 (2002) 9058-9059.

[27] G. Li Puma, Modeling of Thin-Film Slurry Photocatalytic Reactors Affected by Radiation Scattering, Environ. Sci. Tech. 37 (2003) 5783-5791.

[28] J.P. Espinos, J. Morales, A. Barranco, A. Caballero, J.P. Holgado, A.R. Gonzalez-Elipe, Interface Effects for Cu, CuO, and Cu_2O Deposited on SiO_2 and ZrO_2. XPS Determination of the Valence State of Copper in Cu/SiO_2 and Cu/ZrO_2 Catalysts, J. Phys. Chem. B. 106 (2002) 6921-6929.

[29] Y. Li, L. Qin, T. Tang, X. Yao, XPS analysis of $Pb(Zr_{0.52}Ti_{0.48})O_3$ thin film after dry-etching by CHF_3 plasma, Appl. Surf. Sci. 165 (2000) 34-37.

[30] J.B. Umland et al., General Chemistry. 2nd edition. West Publishing, 1996.

[31] Q. Wu, J. Zhao, G. Qin, C. Wang, X. Tong, S. Xue, Photocatalytic reduction of Cr(VI) with TiO_2 film under visible light, Appl. Catal. B. Environ. 142-143 (2013) 142-148.

[32] D.K. Nordstorm, C.N. Alpers, C.J. Ptacek, D.W. Blowes, Negative pH and

Extremely Acidic Mine Waters from Iron Mountain, California, Environ. Sci. Tech. 34 (2000) 254-258.

[33] P.L. Mcarty, J. Bae, J. Kim, Domestic wastewater treatment as a net energy producer – can this be achieved? Environ. Sci. Technol. 45 (2011) 7100-7106.

[34] B.C. O'Regan, J.R. Durrant, Kinetic and energetic paradigms for dye-sensitized solar cells: moving from the ideal to the real, Acc. Chem. Res. 42 (2009) 1799-1808.

[35] Z. Ning, F. Yu, H. Tian, Improvement of dye-sensitized solar cells: what we know and what we need to know, Energy Environ. Sci. 3 (2010) 1170-1181.

[36] D. Wang, Y. Li, G. Li Puma. C. Wang, P. Wang, W. Zhang, Q. Wang, Mechanism and experimental study on the photocatalytic performance of Ag/AgCl@ chiral TiO_2 nanofibers photocatalyst: The impact of wastewater components, J. Hazard. Mater. 285 (2015) 277-284.

[37] C. Lian, D. Jiang, H. Liu, J. Wu, A Generic Model for Electric Double Layer in Porous Electrodes, J. Phys. Chem. C. 120 (2016) 8704-8710.

[38] C. Lina, L. Wang, X. Chen, X. Han, S. Zhao, H. Liu, Y. Hu, Modeling Swelling Behavior of Thermoresponsive Polymer Brush with Lattice Density Functional Theory, Langmuir 30 (2014) 4040-4048.

Graphical Abstract

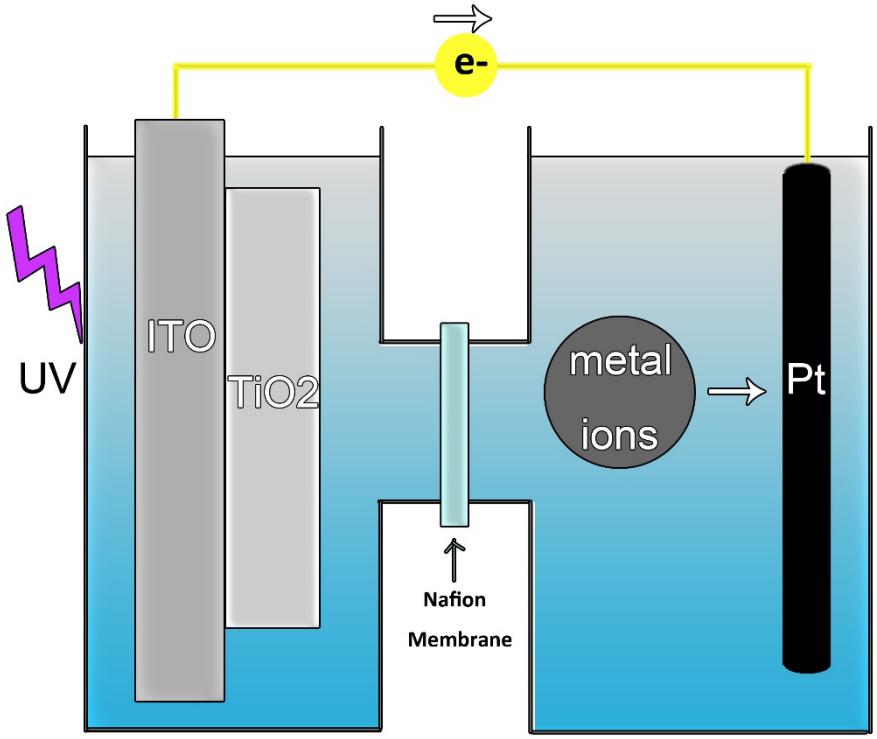

Supplementary Material

Photoelectrochemical Cell for Simultaneous Electricity Generation and Heavy Metals Recovery from Wastewater

Dawei Wang[a], Yi Li[a]*, Gianluca Li Puma[b]*, Panagiotis Lianos[c], Chao Wang[a], Peifang Wang[a],

[a] *Key Laboratory of Integrated Regulation and Resource Development of Shallow Lakes, Ministry of Education, College of Environment, Hohai University. Xi Kang Road #1, Nanjing 210098, PR China; E-mail: wdwhhu@gmail.com*

[b] *Environmental Nanocatalysis & Photoreaction Engineering, Department of Chemical Engineering, Loughborough University, Loughborough LE11 3TU, United Kingdom; E-mail: G.Lipuma@lboro.ac.uk*

[c] *Department of Chemical Engineering, University of Patras, 26500 Patras, Greece*

* Corresponding authors

Crystal size calculation (~3.9 nm)

D = Kλ/(βcos θ), where K is the coefficient (0.9), λ is the X-ray wavelength (1.54056 Å), β is full width at half maximum (FWHM) which is 0.036 rad according the calculation (shown below), θ is 0.224 rad.

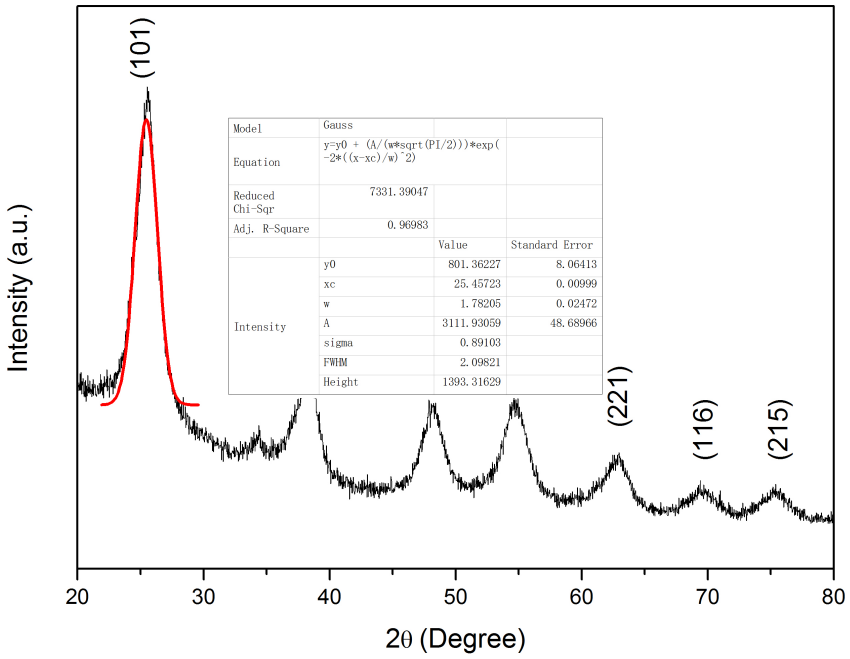

Band gap energy calculation (~3.5 eV)

E = *hC*/λ,

Where *h* is the Plank constant (6.626 10^{-34} Joules*sec), *C* is the speed of light (3 10^{8} m/s), and *λ* is the cutoff wavelength (~394 nm, Fig 2).

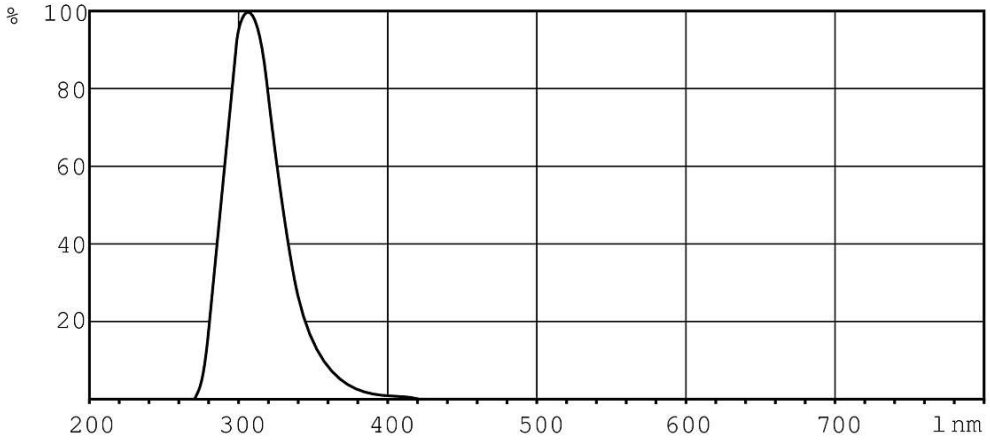

Fig. S1. The emission spectrum of the UV lamp used in the experiment.

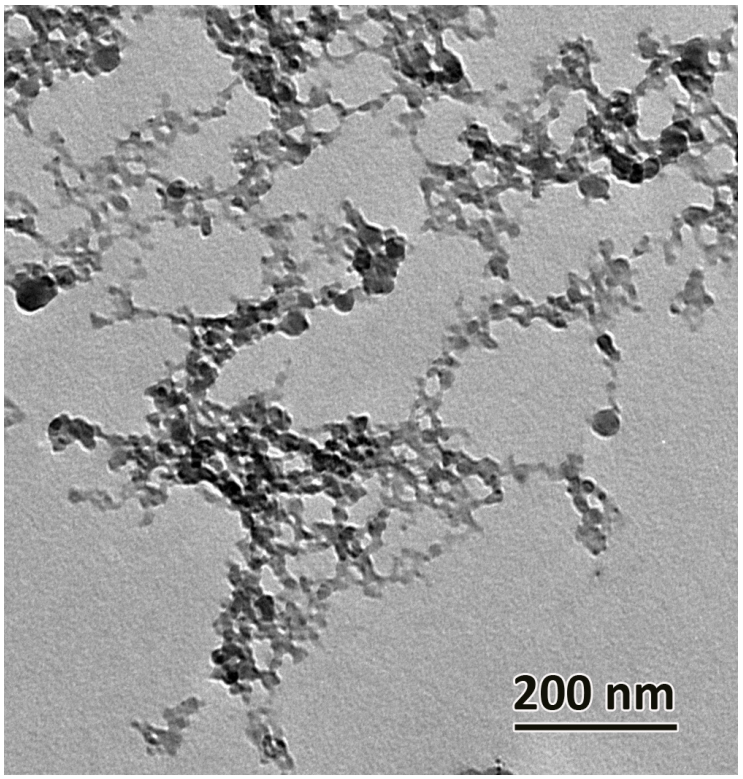

Fig. S2. TEM image of the TiO_2 nanocrystals subject to doctor blade process.

(a)

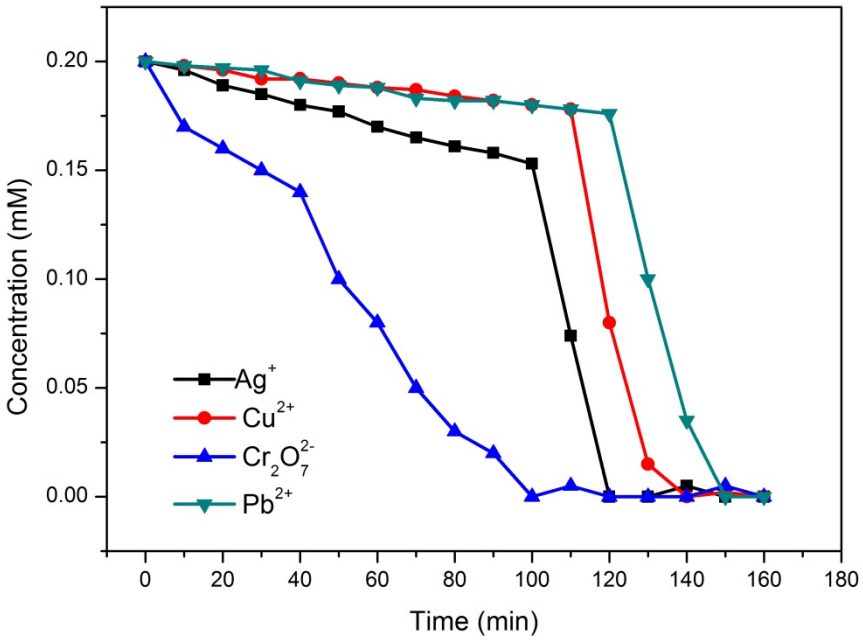

(b)

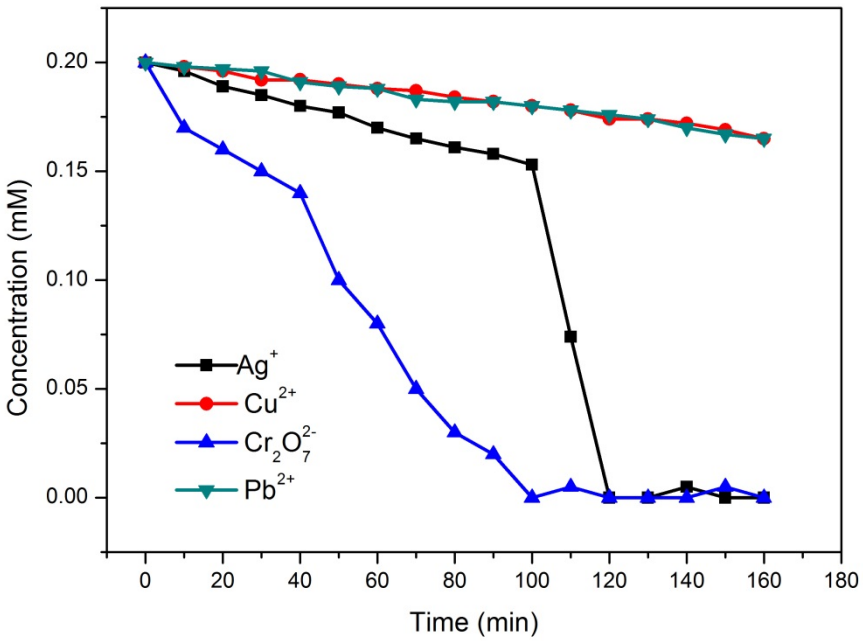

Fig S3. The effect of (a) N_2 and (b) O_2 on the removal of metal ions. The initial concentration of each metal ion was ~0.2 mM and the light intensity was 215 W/m^2.

(a)

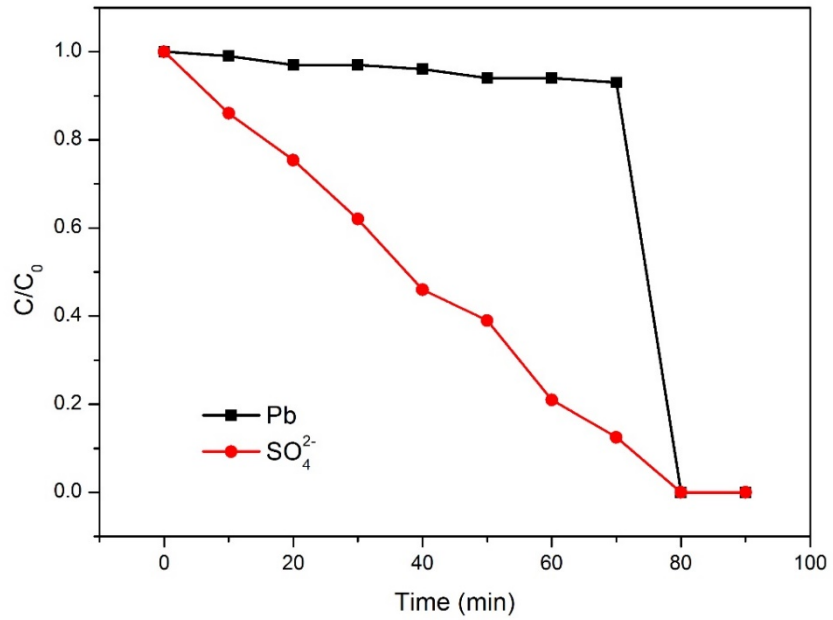

(b)

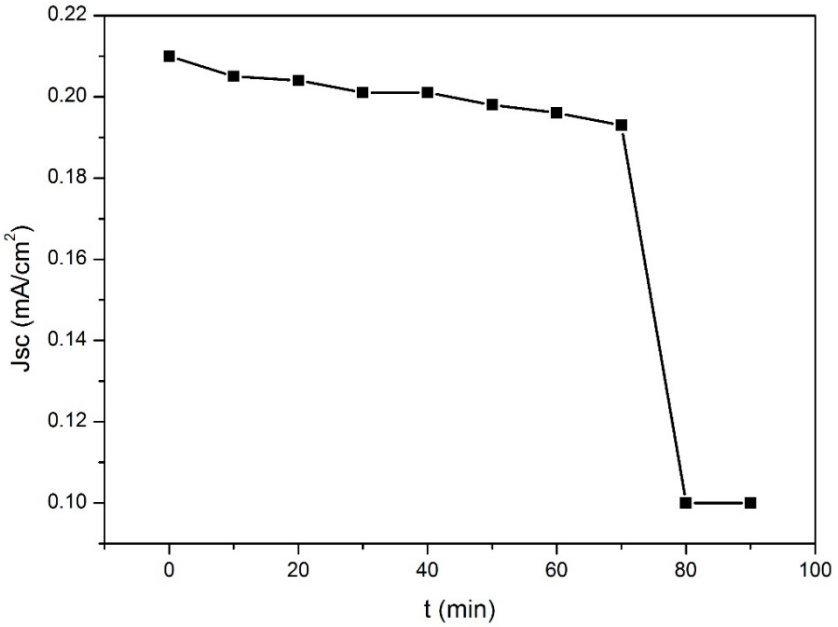

Fig. S4. Artificial wastewater was replaced by the real wastewater from lead-acid battery manufacturing unit, (a) the removal performance of Pb and SO_4^{2-}, and (b) corresponding short current was recorded every 10 min.

(a)

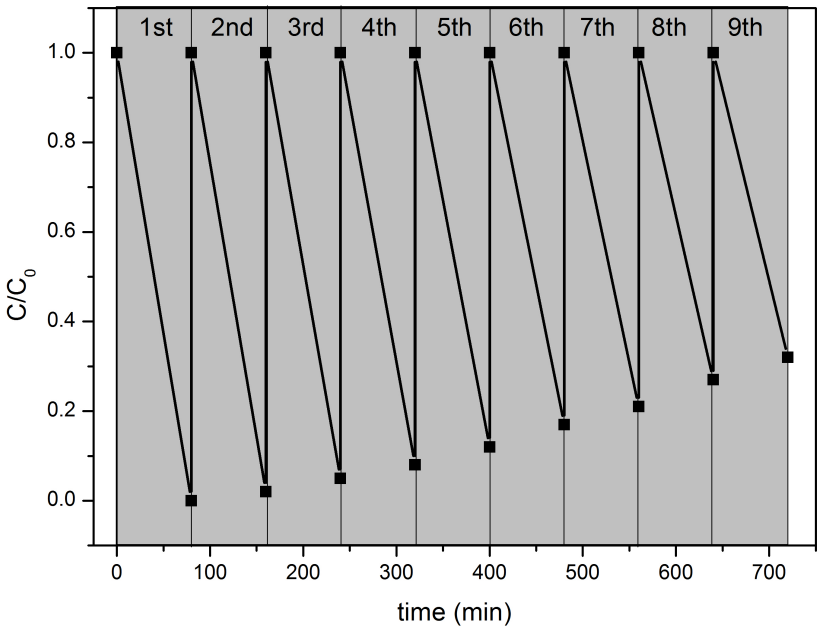

(b)

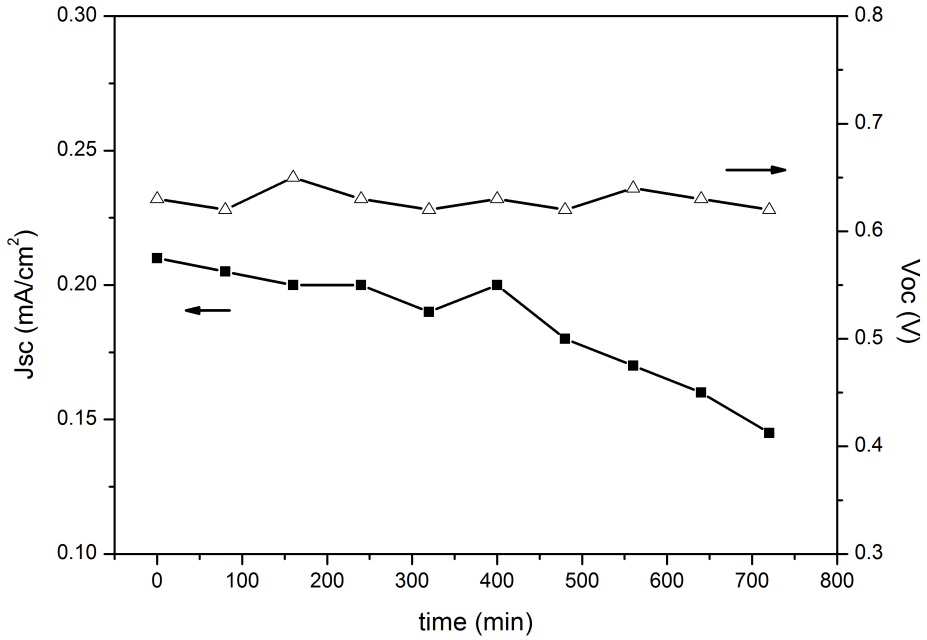

Fig S5. Stability performance of the PEC by applying lead acid battery wastewater, (a) the removal of Pb^{2+} and SO_4^{2-}; (b) *J-V* corresponds to the cycle test in (a).